Pergamon

Int. J. Heat Mass Transfer. Vol. 38, No. 9, pp. 1693–1703, 1995

0017–9310/95 $9.50+0.00

0017-9310(94)00277-0

Prediction of opposing turbulent line jets discharged laterally into a confined crossflow

Y. R. CHANG and K. S. CHEN†

Department of Mechanical Engineering, National Sun Yat-Sen University, Kaohsiung, Taiwan, Republic of China

(*Received* 30 *May* 1994 *and in final form* 8 *August* 1994)

Abstract—A numerical study is presented for the mixing of opposing heated line jets discharged normally or at an angle into a horizontal cold cross-flow in a rectangular channel. The k–ε turbulence model is adopted and the simulation is performed for the jet-to-cross-flow momentum flux ratio ranging from 0.42 to 5.42 and the incident angle from 60° to 90°. The results show that there is a strong recirculation near the downstream region of the nozzle opening, and the temperature field behaves like a deflected plume. The turbulent kinetic energy is high in the region where the vertical velocity gradient is steep. The vertical temperature profiles can be expressed as the self-similar forms. Correlations for the jet temperature and velocity trajectories, the penetration and circulation depths, the jet half-width, and the reattachment point are derived in terms of the momentum flux ratio, the downstream distance and the incident angle. As compared to the case of a one-side line jet, the opposing jets will hinder the vertical penetration but increase the horizontal velocity when the jets impinge on each other. Better thermal mixing can be achieved at higher momentum flux ratio and incident angle.

1. INTRODUCTION

The phenomena of jets discharged normally or at an angle into a confined cross-flow occur in various industrial processes. These include, for example, the effluent operations where streams are mixed for the dilution and the reduction of pollutant formations, and V/STOL aerodynamic lifting or landing. Because of their importance in a variety of applications, several experimental, theoretical and numerical works have been performed where the parameters studied include the jet nozzle shape, the jet incident angle, and jet-to-cross-flow momentum ratio [1, 2]; and the penetration and the mixing characteristics of jets with unconfined cross-flows are of primary concern.

For design considerations in the dilution zone of a gas-turbine combustor, efficient mixing of diluent air entering through the liner holes with high temperature combustion gases leaving the primary zone is desired to provide rapid quenching for any ongoing chemical reaction and a more uniform temperature pattern, which is favorable for the turbine inlet [3]. Experimental investigations have been carried out on the mixing process of the single heated jet injected into a cold cross-flow [4–10] and of the multiple jets injected into a heated crossflow. These studies provided detailed correlations for predicting the temperature distributions and the relevant parametric variations downstream of the jets discharged *normally* from one side into the confined cross-flow.

Numerical study of the mixing of a single jet discharged normally into a cross-flow were done by Patankar *et al.* [11] using a coarse grid system. Jones and McGuirk [12] numerically studied a single round jet in a confined cross-flow and predicted a larger mixing rate than the experimental data of Kamotani and Greber [5], in which the discrepancy was attributed to the diffusion error caused by the coarse grid ($20 \times 15 \times 15$) and to the turbulence model. Holdeman and Srinivasan [13] predicted nonisothermal mixing in a confined cross-flow, where a single row or opposed rows of jets were injected. With the grid system they used, their calculations showed a much lower mixing rate than had been measured.

Most of the previous work is focused on the jets discharged *normally* into the horizontal cross-flow. Recently, Chang and Chen [14, 15] investigated experimentally the effect of the jet incident angle on the mixing of opposing heated line jets with a confined cross-flow. Their results show that better thermal mixing can be achieved at higher jet-to-cross-flow momentum flux ratio and higher incident angle.

This paper presents a numerical investigation of the mixing characteristics of opposing heated line jets with a horizontal cross-flow in a rectangular channel using a turbulent k–ε model. Emphasis is placed on the effects of momentum flux ratio and incident angle on the mixing behavior of lateral jets with the cross-flow. Detailed mean velocity, turbulent kinetic energy and

† Current address: Institute of Environmental Engineering, National Sun Yat-Sen University, Kaohsiung, Taiwan, Republic of China.

NOMENCLATURE

D	jet nozzle width [mm]
H	duct height [mm] (Fig. 1)
I	turbulence intensity $[= (3\overline{u'^2})/(2U_\infty^2)]$
J	momentum flux ratio $[= (\rho_j V_j^2 D/\rho_\infty U_\infty^2 H)]$
k	turbulent kinetic energy $[= 3\overline{u'^2}/2]$
k_∞	inlet turbulent kinetic energy of the crossflow
k_j	inlet turbulent kinetic energy of the jet
M_R	reverse flow rate intensity defined in equation (15)
P	pressure
P_r	Prandtl number, $= \nu/\alpha$
T	mean temperature
T_j	mean jet temperature at the nozzle opening
T_∞	crossflow inlet temperature
U_∞	crossflow inlet velocity
U	mean horizontal velocity
$\tilde{U}$	velocity difference ratio defined in equation (14)
u_*	friction velocity $[= \sqrt{\tau_w/\rho}]$
$\overline{u_j'}$	root-mean-square component of horizontal turbulent velocity
V_j	mean jet velocity at the nozzle opening
$\overline{v_j'}$	root-mean-square component of jet turbulent velocity at nozzle opening
$W_{1/2}^{\pm}$	plus or minus jet half-width (Fig. 2)
X	horizontal coordinate (Fig. 1)
X_R	reattachment point or length of circulation zone (Fig. 2)
Y	vertical coordinate (Fig. 1)
Y_c	velocity zero-crossing point or jet circulation depth (Fig. 2)
Y_T	jet thermal penetration depth (Fig. 2)
Y_v	jet velocity penetration depth (Fig. 2)
y^+	local Reynolds number $[= Yu_*/\nu]$
Z	spanwise direction (Fig. 2).

Greek symbols

α	thermal diffusivity of air
ε	turbulent dissipation energy
θ	temperature difference ratio defined in equation (13)
κ	Von Karman constant ($= 0.4187$)
λ_∞	a length scale factor for crossflow ($= 0.003$)
λ_j	a length scale factor for jet ($= 0.015$)
μ	dynamic viscosity of fluid
μ_t	turbulent viscosity
ν	kinematic viscosity of fluid $[= \mu/\rho]$
ν_t	turbulent kinematic viscosity $[= \mu_t/\rho]$
ρ_∞	density of crossflow at inlet
ρ_j	jet density at nozzle opening
σ	percentage root-mean-square deviation
σ_ε	constant in turbulent ε-equation ($= 1.3$)
σ_k	constant in turbulent k-equation ($= 1.0$)
τ_w	shear stress at the wall
ϕ	jet incident angle.

temperature fields are presented, and correlations of parametric variations such as the velocity and temperature trajectories, the circulation depth and length are examined and discussed.

2. THEORETICAL FORMULATIONS

2.1. *The governing equations*

Consider the in-line opposing heated jets discharged at an angle ϕ into a horizontal crossflow in a rectangular channel, as is shown in Fig. 1. For a steady, two-dimensional, incompressible, turbulent flow with constant fluid properties, the governing equations written in the Cartesian tensor notations are as follows:

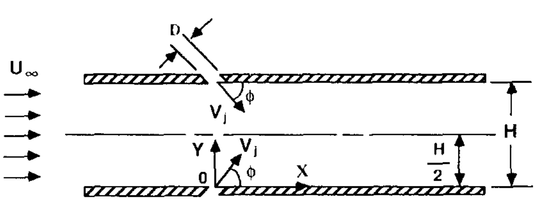

Fig. 1. Schematic of physical model and coordinate system.

$$\frac{\partial U_i}{\partial X_i} = 0 \tag{1}$$

$$\frac{\partial(\rho U_i U_j)}{\partial X_j} = \frac{\partial(-\rho\overline{u_i'u_j'})}{\partial X_j} - \frac{\partial P}{\partial X_i} + \frac{\partial}{\partial X_j}\left\{\mu\left(\frac{\partial U_i}{\partial X_j} + \frac{\partial U_j}{\partial X_i}\right)\right\} \tag{2}$$

$$\frac{\partial(\rho U_j T)}{\partial X_j} = \frac{\partial(-\rho\overline{u_j'T'})}{\partial X_j} + \frac{\partial}{\partial X_j}\left\{\mu\frac{\partial T}{\partial X_j}\right\}. \tag{3}$$

In the above, U_i and T are the mean velocity and temperature, u_i' and T' are the corresponding fluctuation components; and $\overline{u_i'u_j'}$ and $\overline{u_j'T'}$ are the averaged Reynolds stresses and turbulent heat fluxes, respectively.

Closure of equations (1)–(3) is by means of the k–ε turbulence model, for which the additional equations are:

$$\overline{u_i'u_j'} = -\nu_t\left(\frac{\partial U_i}{\partial X_j} + \frac{\partial U_j}{\partial X_i}\right) \tag{4}$$

$$\nu_t = C_\mu k^2/\varepsilon \tag{5}$$

$$-\overline{u_j'T'} = \nu_t \frac{\partial T}{\partial X_j} \tag{6}$$

$$U_j \frac{\partial k}{\partial X_j} = \nu_t \left(\frac{\partial U_i}{\partial X_j} + \frac{\partial U_j}{\partial X_i}\right)\frac{\partial U_i}{\partial X_j} + \frac{\partial}{\partial X_j}\left(\frac{\nu_t}{\sigma_k}\frac{\partial k}{\partial X_j}\right) - \varepsilon \tag{7}$$

$$U_j \frac{\partial \varepsilon}{\partial X_j} = C_1 \nu_t \frac{\varepsilon}{k}\left(\frac{\partial U_i}{\partial X_j} + \frac{\partial U_j}{\partial X_i}\right)\frac{\partial U_i}{\partial X_j} + \frac{\partial}{\partial X_j}\left(\frac{\nu_t}{\sigma_\varepsilon}\frac{\partial \varepsilon}{\partial X_j}\right) - C_2 \frac{\varepsilon^2}{k}. \tag{8}$$

In the above, k and ε are the turbulent kinetic energy and turbulent dissipation, respectively. In this work, the standard set of constants are adopted for the above equations according to [16]:

$$C_\mu = 0.09 \quad C_1 = 1.44 \quad C_2 = 1.92$$

$$\sigma_k = 1.0 \quad \sigma_\varepsilon = 1.3.$$

2.2. *Details of modeling*

As is shown in Fig. 1, the origin O is at the nozzle opening of the bottom jet. The top and bottom walls are impermeable and adiabatic, with vanishing fluid velocity. The inlet conditions of turbulent kinetic energy and turbulent dissipation for the horizontal cross-flow are given by

$$k_\infty = I_\infty U_\infty^2 \tag{9}$$

$$\varepsilon_\infty = k_\infty^{3/2}/(\lambda_\infty H) \tag{10}$$

where U_∞ is the bulk mean inflow velocity, I_∞ is the inflow turbulent intensity, H is the channel height, and λ_∞ is the length scale factor.

Similarly, the inlet conditions of turbulent kinetic energy and dissipation for the opposing line jets are:

$$k_j = I_j V_j^2 \tag{11}$$

$$\varepsilon_j = k_j^{3/2}/(\lambda_j D) \tag{12}$$

where V_j and I_j are the inflow mean velocity and turbulent intensity of the jets, D is the nozzle width, and λ_j is the corresponding length scale factor.

Following the approach of Tennekes and Lumley [17], the length scale factors of λ_∞ and λ_j were tuned to obtain the best fit with the available data. Accordingly, all results presented in this paper are obtained by setting $\lambda_\infty = 0.003$ and $\lambda_j = 0.015$ in equations (10) and (12), respectively. Note that the uniform velocity and temperature profiles for the horizontal cross-flow are specified as the inlet boundary conditions at the upstream location $X/D = -20$, while the zero-gradient fluxes are assumed as the outlet boundary conditions at the far downstream location $X/D = 80$.

The region close to the wall is the one where the local Reynolds number y^+ (based on the friction velocity $u_* = \sqrt{\tau_w/\rho}$ and the distance Y from the wall) changes considerably. The approach in this work is such that a laminar sublayer is assumed for $y^+ \leqslant 11.63$ [18, 19], in which turbulent kinetic energy k vanishes while turbulent dissipation ε reaches its highest value according to $\varepsilon_p = C_\mu^{3/4} k_p^{3/2}/\kappa y_p$ [18]. Note that the subscript p denotes the quantity at the calculation nodal point next to the wall. The flow is assumed completely turbulent for $y^+ \geqslant 11.63$. It should be noticed that, although the k–ε model is widely used for predicting flow interaction between jets and crossflow [11, 16], it is generally realized that the isotropy assumption in the k–ε model is not valid in the reversed flow region. In a comprehensive review by Sloan *et al.* [20], it was pointed out that the k–ε model is poor in the reversed flow region, but satisfactory in predictions in the recovery region (outside the reverse flow region). Further, other versions, such as the algebraic stress model (ASM), have the drawback that the constants have not been optimized and the superiority of the ASM in different regions of complicated flow is not conclusive. In this study, the mixing of lateral jets and crossflow, which is out of the recirculation zone, is the main concern. Therefore, the application of the k–ε model

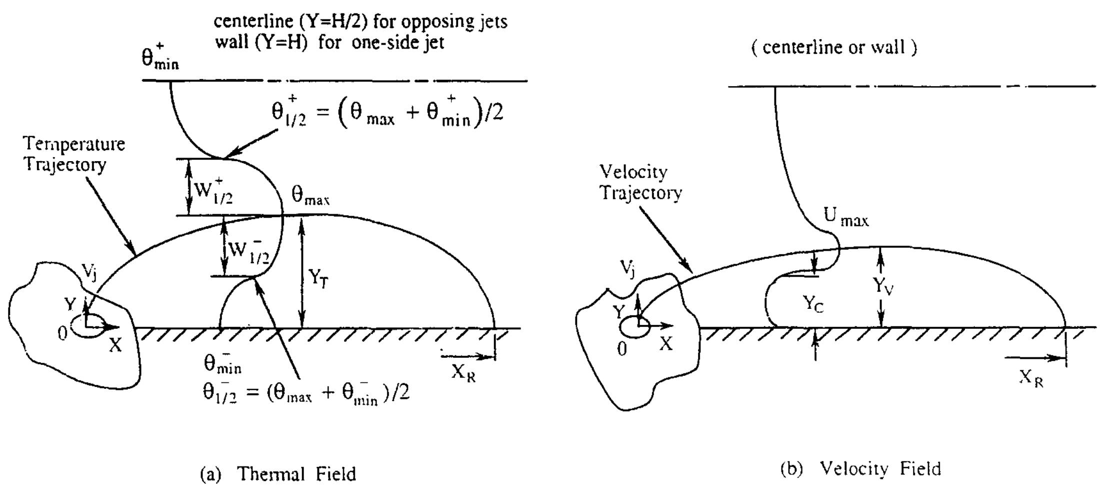

Fig. 2. Parameters characterizing the temperature and velocity profiles.

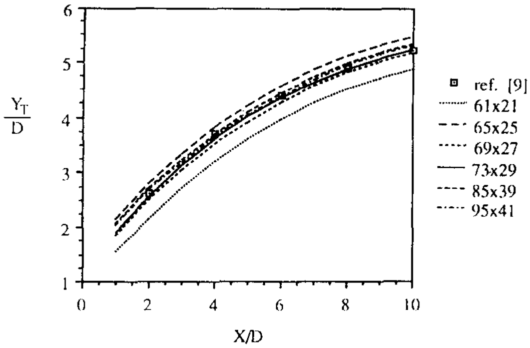

Fig. 3. Validation tests for various grid system ($J = 0.83$, $\phi = 90^\circ$).

to the problem appears acceptable and can serve as a basis for future comparison with other models.

3. NUMERICAL SIMULATIONS

Equations (1)–(8) are solved by the control-volume-based finite difference formulation and by the SIMPLE calculation procedures in conjunction with the successive under-relaxation method [19]. A non-uniform grid system was employed in the calculation domain with fine grid spacings near the jet openings and the channel walls. Due to the symmetrical flow characteristics for the case of opposing in-line jets [9, 15], only the lower half ($0 \leqslant Y/H \leqslant 0.5$) of the entire domain was calculated. Note that some results for the case of one-side line jet were also presented, in which no symmetrical condition was assumed. Prior to the calculations, tests were conducted by comparing the results obtained among the various grid spacings and with the experimental data for the opposing in-line jets at $\phi = 90^\circ$ [9]. These are summarized in Fig. 3, where it shows that the solutions converge when the grid spacing is refined. To achieve a reasonable accuracy within a moderate computing time, most results presented in this paper were obtained using a 73×29 grid system for the opposing in-line jets, and a 73×45 grid system for the one-side line jet.

Numerical simulations were carried out for a fixed $H/D = 24$ (ratio of channel height to nozzle width) and $Pr = 0.711$ (for air) over the ranges of $0.42 \leqslant J \leqslant 5.42$, $60^\circ \leqslant \phi \leqslant 90^\circ$, and $-20 \leqslant X/D \leqslant 80$, as is shown in Table 1. Notice that in the present notation, the ratio of D over $H(D/H)$ has been included in defining the momentum flux ratio J. In addition, only the variables of momentum flux ratio J, downstream distance X/D, and jet incident angle ϕ are used as the independent parameters in data reduction, but others such as ρ_j/ρ_∞ are not considered due to the limited range of variation. The results for the temperature and velocity profiles are normalized as the difference ratios with respect to their inlet conditions according to:

$$\theta = \frac{T - T_\infty}{T_j - T_\infty} \tag{13}$$

$$\tilde{U} = \frac{U - U_\infty}{U_{max} - U_\infty} \tag{14}$$

where U_{max} is the maximum velocity at a given cross-section.

The relevant parameters characterizing the mixing processes of one-side jet or opposing line jets discharging into a cross-flow are depicted in Fig. 2, where it shows the jet temperature trajectory Y_T, the jet velocity trajectory Y_v, the recirculation depth Y_c, etc. Note that the mixing characteristics of the flow can also be represented by the momentum difference ratio, the so-called *reverse flow rate intensity* M_R according to [21]:

$$M_R = \frac{\int \rho(|U| - U)\,dY}{M_j + M_\infty} \tag{15}$$

where M_j and M_∞ are the mass flow rates of jet and cross-flow, respectively. It is seen that, if there is no recirculation zone or outside it, then $|U|$ is equal to U and M_R in above equation would vanish. However, the numerator and M_R in above equation would be positive inside the recirculation zone. Further, for fixed inflow conditions (e.g. M_j and M_∞ are constant), larger values in the numerator of equation (15) means a larger recirculation mass flow rate. It follows that larger value of M_R corresponds to a stronger recirculation and longer mixing time; thus, better mixing can be achieved.

The convergence criteria for each control volume were that the maximum residuals of the mass, momentum and energy were all less than 1.0×10^{-3} and the maximum relative errors of the velocity components were less than 1.0×10^{-5}. The computation time was approximately 6100–8100 s for a 73×29 grid system on a CDC Cyber 180/840A NOS/VE; and was about 7200–9600 s for a 73×45 grid system.

4. RESULTS AND DISCUSSION

4.1. *Velocity vectors and isotherm contours*

Figures 4–6 show the velocity vectors and the isotherms of the mean flow for different momentum flux ratios J and incident angle ϕ. It is seen from these figures that, when the jet merges with the crossflow, there is a circulation zone near the downstream region of the nozzle opening. The isotherms exhibit a deflected plume, and the temperature of the merged flow becomes more and more uniform as the fluid moves downstream. When Figs. 4 and 5 are compared, it is seen that the recirculation size becomes larger and the isotherms move away from the jet side as the incident angle ϕ increases. That is, better mixing can be achieved at a higher incident angle. A similar trend is also found for a higher momentum flux ratio when comparison is made between Figs. 4 and 6.

Typical flow and thermal fields for the case of a one-side line jet is illustrated in Fig. 7 at $J = 1.25$ and $\phi = 90^\circ$. When compared with the case of the opposing jets in Fig. 5, the results show that the pen-

Table 1. Conditions for numerical simulation

ϕ	T_j [°C]	T_∞ [°C]	V_j [m s^{-1}]	U_∞ [m s^{-1}]	ρ_j/ρ_∞	J	I_j	I_r
60°	60	24	9.103	2.37	0.898	0.42	0.03	0.007
			11.223			0.83	0.03	0.007
			13.745			1.25	0.0299†	0.008†
			15.871			1.67	0.03	0.007
			17.745			2.08	0.03	0.007
			19.438			2.5	0.0299†	0.074†
			20.996			2.92	0.03	0.007
			22.445			3.33	0.03	0.0076
			23.807			3.75	0.03	0.007
			25.095			4.17	0.03†	0.0071†
			28.612			5.42	0.03	0.0076
75°	81	25	11.925	3.460	0.842	0.42	0.0299	0.0051
			11.210	2.300		0.83	0.03	0.0061
			11.969	2.005		1.25	0.03	0.0065
			11.786	1.710		1.67	0.03†	0.0067†
			12.076	1.567		2.08	0.03	0.0065
			12.013	1.423		2.5	0.0299†	0.007†
			11.990	1.230		3.33	0.0299	0.007
			11.989	1.100		4.17	0.03†	0.0064†
			11.939	1.000		5.0	0.03	0.0067
90°	81	25	11.925	3.460	0.842	0.42	0.03	0.006
			11.210	2.300		0.83	0.03	0.006
			12.004	2.203		1.04	0.031†	0.0062†
			11.969	2.005		1.25	0.031†	0.0059†
			11.786	1.710		1.67	0.03	0.006
			12.076	1.567		2.08	0.031†	0.0057†
			12.013	1.423		2.5	0.03	0.006
			11.990	1.230		3.33	0.03	0.006
			11.989	1.100		4.17	0.03	0.006
			11.939	1.000		5.0	0.03	0.006

† Data taken from refs. [9, 14, 15].

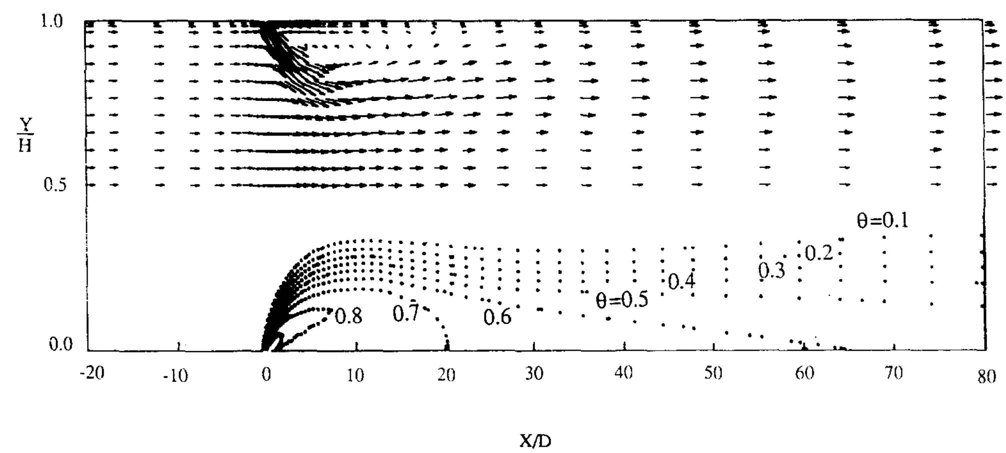

Fig. 4. Velocity vectors and isotherms of opposing in-line jets at $J = 1.25$ and $\phi = 60°$.

etration of a single jet is much deeper than that of the opposing jets under otherwise similar conditions. This is due to the fact that the squeeze of vertical velocity around the impingement point will hinder the vertical penetration. Meanwhile, local pressure and horizontal velocity would increase, partly due to the conversion of vertical momentum and partly due to the mass continuity requirement. Further, isotherm contours show that temperature would be more uniform for the opposing jets than for the one-side jet.

4.2. *Vertical velocity profiles*

Figure 8(a) and (b) shows the vertical velocity profiles of the mean flow at various cross-sections for $J = 1.25$, $\phi = 60°$, and $J = 1.25$, $\phi = 90°$. The results show that the horizontal velocity at each station increases from the wall with height to a maximum value U_{max}, above which it decreases to a minimum value at the channel mid-height ($Y/H = 0.5$). Notice that the location Y_v, where $U = U_{max}$ at each station, is the so-called *jet velocity trajectory*. Because there is

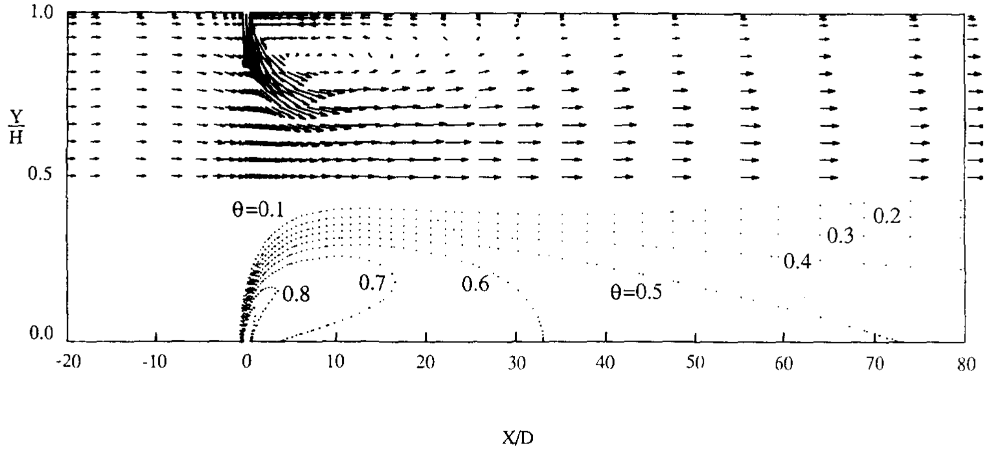

Fig. 5. Velocity vectors and isotherms of opposing in-line jets at $J = 1.25$ and $\phi = 90^\circ$.

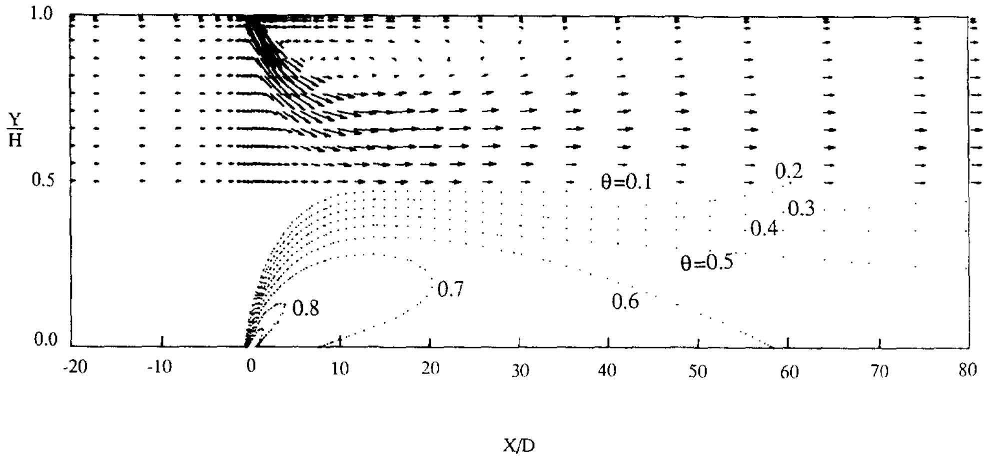

Fig. 6. Velocity vectors and isotherms of opposing in-line jets at $J = 4.17$ and $\phi = 60^\circ$.

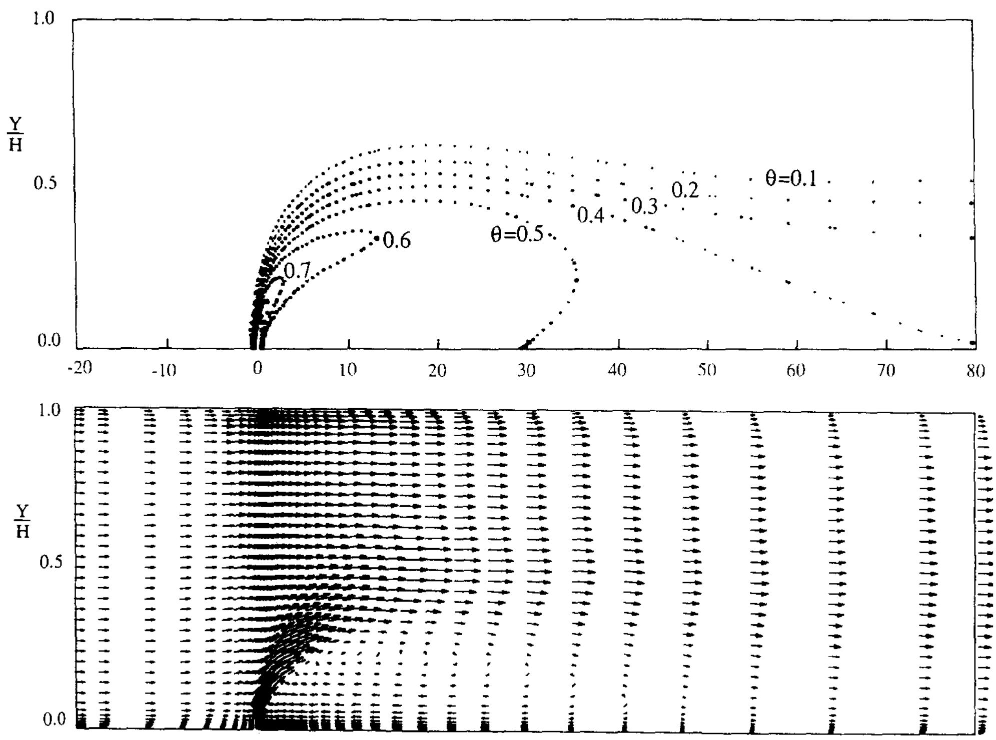

Fig. 7. Velocity vectors and isotherms of one-side line jet at $J = 1.25$ and $\phi = 90^\circ$.

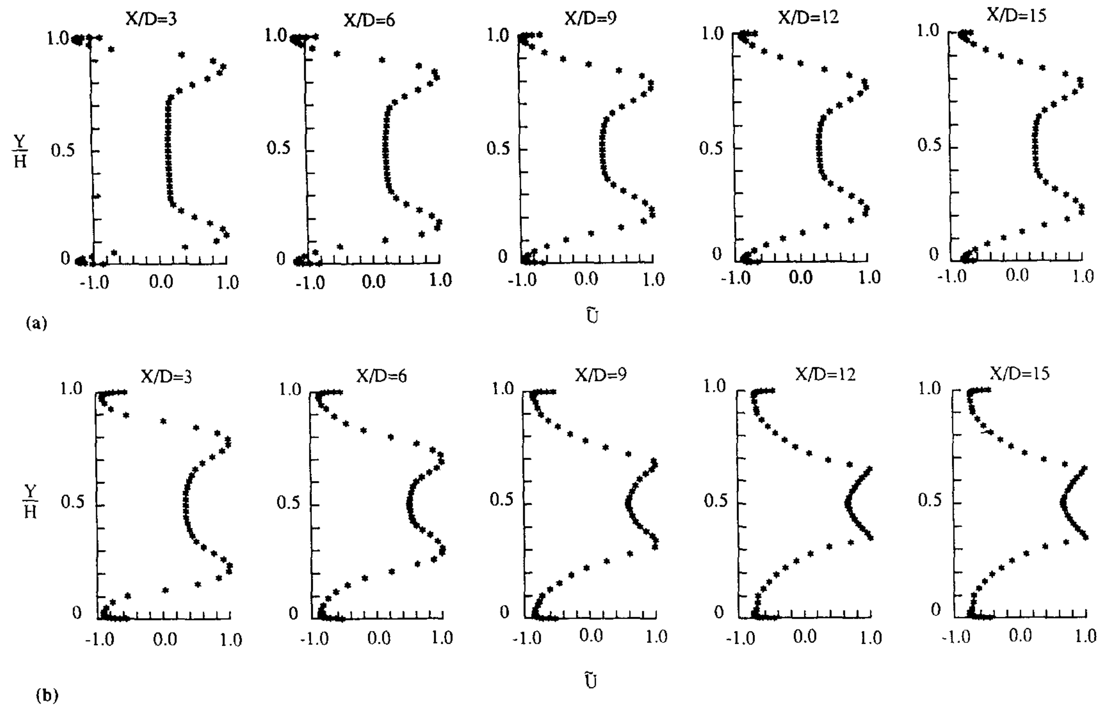

Fig. 8. Vertical velocity profiles of opposing in-line jets at: (a) $J = 1.25$, $\phi = 60^\circ$; and (b) $J = 1.25$, $\phi = 90^\circ$.

Table 2. Correlation equations for opposing line jets

Y_T/D	$0.797J^{0.274}(X/D)^{0.395}\sin\phi^{3.445}$	$\sigma = \pm 9.7\%$
$\theta^{+}_{min}/\theta_{max}$	$1-e^{-C^{+}}$	$\sigma = \pm 11.1\%$
	$C^{+} = 5.23\times 10^{-12}J^{2.572}(X/D)^{3.331}\sin\phi^{13.19}$	
$\theta^{-}_{min}/\theta_{max}$	$1-e^{-C^{-}}$	$\sigma = \pm 6.6\%$
	$C^{-} = 2.147J^{-0.075}(X/D)^{0.198}\sin\phi^{-0.944}$	
$W^{+}_{1/2}/D$	$1.497J^{0.135}(X/D)^{0.132}\sin\phi^{-0.378}$	$\sigma = \pm 7.4\%$
$W^{-}_{1/2}/D$	$0.427J^{0.166}(X/D)^{0.429}\sin\phi^{2.866}$	$\sigma = \pm 12.3\%$
Y_v/D	$1.751J^{0.180}(X/D)^{0.365}\sin\phi^{2.503}$	$\sigma = \pm 6.5\%$
Y_c/D	$0.580J^{0.127}(X/D)^{0.676}\sin\phi^{3.248}$	$\sigma = \pm 8.2\%$
X_R/D	$10.655J^{0.304}\sin\phi^{2.052}$	$\sigma = \pm 1.7\%$

a recirculation zone, the results show that the velocity difference ratio $\tilde{U}$ [defined in equation (14)] at a given cross-section is negative near the jet side. But there is a zero-crossing point Y_c (the so-called *jet circulation depth*) from which $\tilde{U}$ changes from a negative value to a positive one. It is seen from Fig. 8(a) and (b) that both Y_v and Y_c increase with the incident angle ϕ and the downstream distance. The correlation equations for Y_v and Y_c derived from the calculation data are listed in Table 2. Figure 9 shows the typical correlation curves and calculation data of Y_v for various J and X/D at $\phi = 75^\circ$.

When the recirculation occurs in the flow, the reverse flow rate intensity M_R defined in equation (15) is not equal to zero and a larger value of M_R implies a stronger mixing effect. Figure 10 shows the distributions of M_R vs X/D for varying momentum flux ratio J at $\phi = 75^\circ$. It is seen from Fig. 10 that, for a fixed J, the reverse flow rate intensity increases first with the downstream distance to a maximum value and then decreases thereafter. It also shows that M_R increases with increasing momentum flux ratio J. Notice that, for a given condition of J and ϕ, there is a non-trival zero value of X/D for every curve in Fig. 10 that defines the *reattachment point* X_R of the recirculation zone. It is seen from Fig. 10 that X_R also increases with increasing momentum flux ratio J. The correlation equation for X_R derived from the calculation data is listed in Table 2, which shows that better mixing can be achieved at higher momentum flux ratio and incident angle.

4.3. *Turbulent kinetic energy*

Typical distribution of turbulent kinetic energy is depicted in Fig. 11 for $J = 1.25$ and $\phi = 90^\circ$. It is seen from Fig. 11 that the turbulent kinetic energy is high in the region where the mean velocity gradient is steep (see Fig. 5) and the peak value ($k/V_j^2 = 0.38$) occurs at the location $X/D \simeq 13.6$ and $Y/H \simeq 0.38$. The tur-

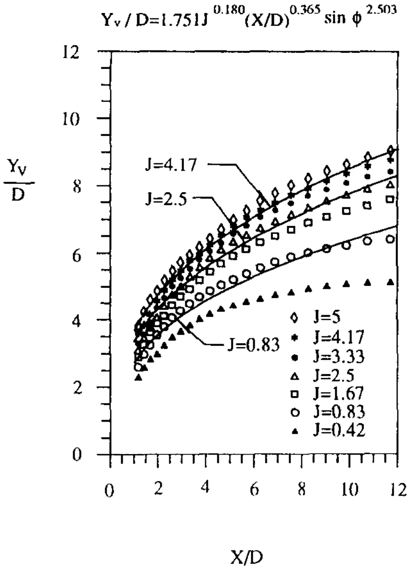

Fig. 9. Velocity trajectories of opposing in-line jets at $\phi = 75°$.

bulent kinetic energy decreases after the peak value and becomes more and more uniform far downstream.

4.4. *Vertical temperature profiles*

Typical vertical temperature profiles are shown in Fig. 12(a) and (b) for the one-side jet and the opposing line jets, respectively, at $J = 1.25$ and $\phi = 90°$. The results show that, at each cross-section, the temperature of the flow increases from the nozzle opening with the height to a maximum value, above which it drops quickly to a minimum value at the channel mid-height $Y/H = 0.5$. Notice that the position of the maximum temperature at a given cross-section is the so-called the *penetration depth* or the *jet temperature trajectory*, Y_T. It is seen that the temperature trajectory Y_T increases with the increasing downstream distance X/D.

Previous works by Holdeman and Walker [7] and Chen and Hwang [9] for one-side jets discharged normally ($\phi = 90°$) into the cross-flow have shown the

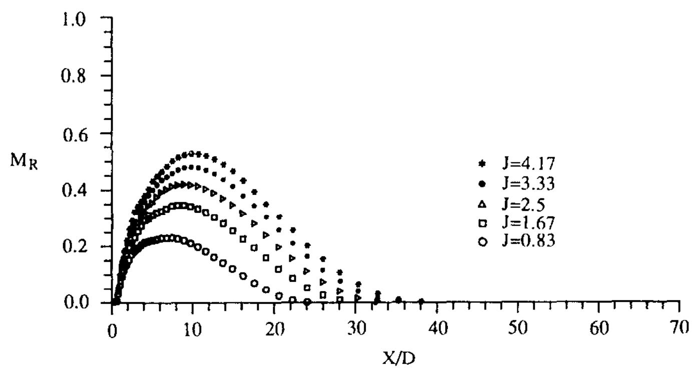

Fig. 10. Reverse flow rate intensity profiles of opposing in-line jets at $\phi = 75°$.

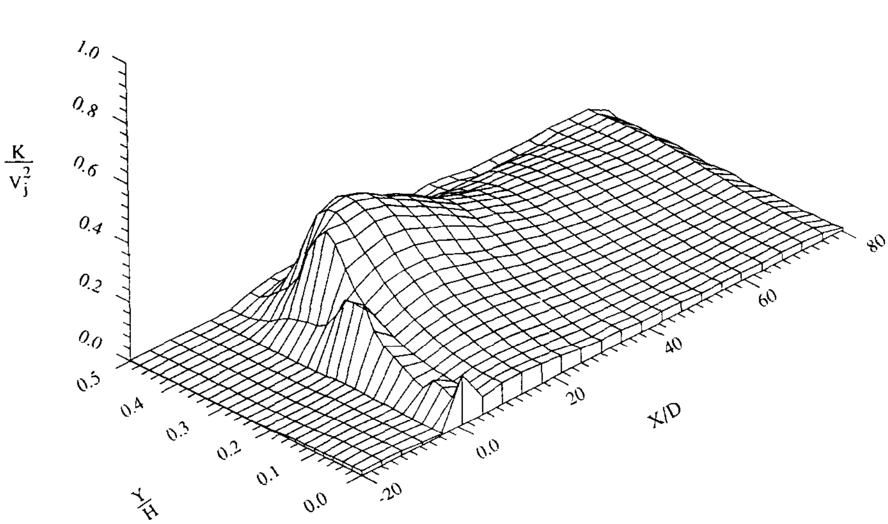

Fig. 11. Turbulent kinetic energy distribution at $J = 1.25$ and $\phi = 90°$.

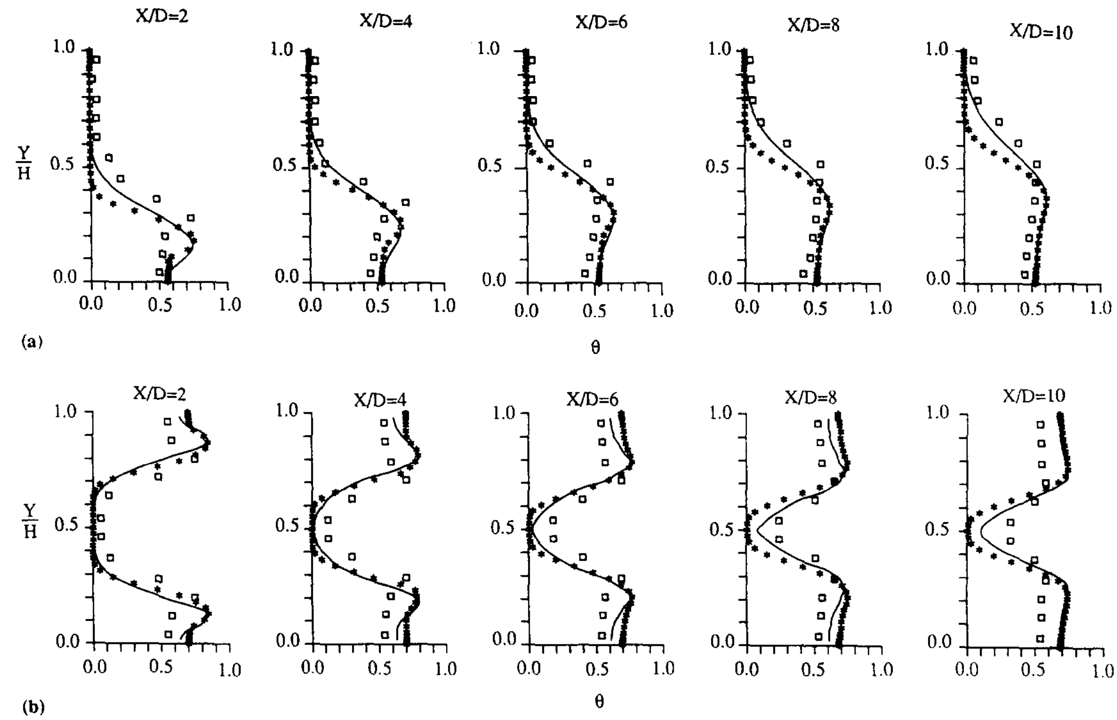

Fig. 12. Vertical temperature profiles at $J = 1.25$, $\phi = 90°$ for: (a) one-side line jet; and (b) opposing in-line jets. (——) Equation (16); (*) calculation; (□) data from refs. [9, 15].

existence of locally self-similar forms for the vertical temperature profiles. These have also been found in the recent work by Chang and Chen [14, 15], taking the incident angle into accounts. The self-similar form of the vertical temperature profiles for the one-side and opposing line jets can be cast into the following form:

$$\frac{\theta-\theta^{\pm}_{\min}}{\theta_{\max}-\theta^{\pm}_{\min}} = A1 \cdot \exp\left\{-A2\left(\frac{Y/H-Y_T/H}{W^{\pm}_{1/2}/H}\right)^2\right\}\cdot(\sin\phi)^{A3}. \quad (16)$$

In the above $A1$, $A2$ and $A3$ are constants and the minus sign refers to the jet side, while the plus sign refers to that side away from the jet. The above three constants can be derived from the data fitting and are summarized in Table 3. Equation (16) is also plotted as the solid lines in Fig. 12(a) and (b), where the measurement data from refs. [9, 15] and the present results are also shown. Several remarks are given below. First, the percentage root-mean-square deviation (σ) of equation (16) from the calculation data is within 9%. Secondly, numerical prediction agrees fairly well with the experimental data, though some discrepancy still exists. This is mainly due to the fact that an adiabatic wall condition was assumed in the computation ($\partial\theta/\partial Y = 0$ at $Y = 0$), but there were some heat losses from the walls in the experiments [9, 15]. Thus, it can be seen from Fig. 12(a) and (b) that the computation overestimates somewhat the mean temperatures near the wall. At meanwhile, since symmetry boundary conditions at $Y/H = 0.5$ were implemented in the calculations, it would result in the underestimate of the jet temperature trajectory Y_T. This is due to the fact that a local high pressure around the impingement point will hinder the vertical penetration as described previously.

Table 3. Values of $A1$, $A2$ and $A3$ in equation (16)

	$A1$	$A2$	$A3$	ϕ
One-side line jet	1.15	0.4	1.825	60–90°
Opposing line jets	1.031	0.622	0.213	60–90°

Other dependent parameters characterizing the thermal mixing of the opposing line jets with the cross-flow can also be obtained from the calculation results. These include the jet temperature trajectory Y_T, the plus- and minus-minimum temperature $\theta^{\pm}_{\min}$, and the jet half-width $W^{\pm}_{1/2}$, as depicted in Fig. 2. The resulting correlations derived from the calculation results are summarized in Table 2 in terms of the independent variables J, ϕ and X/D. Typical correlation curves for the jet temperature trajectory are presented in Fig. 13, and appear to be parabolic lines ($Y_T \propto X^{0.395}$). Table 2 also shows that the jet half-width $W^{\pm}_{1/2}$ increases with increasing J, X/D and ϕ.

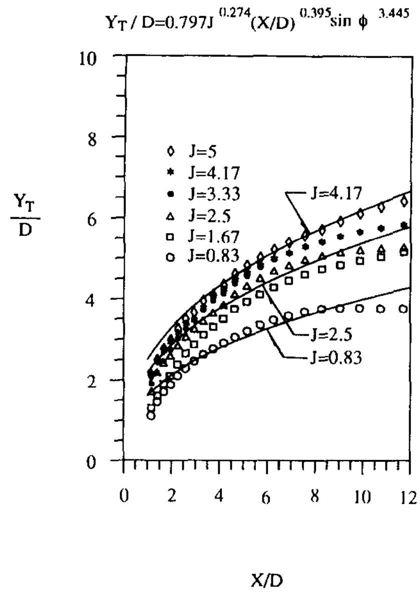

Fig. 13. Temperature trajectories of opposing in-line jets at $\phi = 75°$.

5. CONCLUSIONS

The behavior of opposing heated line jets discharged normally or at an angle into a confined crossflow is studied numerically by means of the turbulent k–ε model. Calculations were carried out for a range of $0.42 \leqslant J \leqslant 5.42$, and $60° \leqslant \phi \leqslant 90°$ at a fixed channel-height to nozzle width $H/D = 24$. Except for some minor discrepancy that is due to the inadequacy of the imposed boundary conditions, the calculation results compare fairly well with the available experimental data. Correlation equations for various parameters characterizing the mixing effect are derived and presented.

Velocity vectors of the mean flow show that there is a recirculation zone down-stream of the jet opening. The jet velocity trajectory, the circulation depth, the circulation length (or the reattachment point) and the reverse flow rate intensity all increase with increasing momentum flux ratio, incident angle, and/or the downstream distance. The turbulent kinetic energy is high in the region where the vertical velocity gradient is high. Turbulent kinetic energy decreases after the peak value and become more uniform far downstream.

The isotherms of the mean flow exhibit a deflected plume and the vertical temperature profiles can be expressed in the self-similar forms. The jet temperature trajectory, the plus- and minus-temperatures and jet half-widths are all increasing with increasing momentum flux ratio, incident angle and downstream distance.

As compared to the case of one-side line jet, the opposing jets would result in higher turbulent kinetic energy and better thermal mixing effects. That is, a more uniform temperature profile can be achieved in a shorter distance by the opposing jets, especially at higher momentum flux ratio and incident angle. This is important, for example, in the design of dilution zone length in the gas-turbine combustors, in which the size and the cost of the combustion chamber can be reduced. It is believed that even better mixing can be achieved if opposing jets are set in different streamwise locations, which deserves further invstigation.

Acknowledgement—Partial support of this work by the National Science Council in Taiwan under grant NSC-82-0401-E-110-034 is acknowledged.

REFERENCES

1. J. A. Schetz, Injection and mixing in turbulent flow, *Prog. Astronaut. Aeronaut.* **68,** 111–164 (1980).
2. S. A. Sherif and R. H. Pletcher, Measurements of the thermal characteristics of heated turbulent jets in crossflow, *ASME J. Heat Transfer* **111,** 897–903 (1989).
3. A. H. Lefebvre, *Gas Turbine Combustor*, pp. 107–137. Hemisphere, Washington, DC (1983).
4. E. E. Callagan and R. S. Ruggeri, A general correlation temperature profile downstream of a heated air jet directed perpendicular to the air stream, NACA TN-2466 (1951).
5. Y. Kamotani and I. Greber, Experiments on a turbulent jet in a cross flow, *AIAA J.* **10,** 1425–1429 (1972).
6. G. B. Cox Jr, Multiple jet correlations for gas turbine engine combustor design, *ASME J. Engng Power* **98,** 265–273 (1976).
7. J. D. Holdeman and R. E. Walker, Mixing of a row of jets with a confined crossflow, *AIAA J.* **15,** 243–249 (1977).
8. J. Andreopoulos, Measurements in jet-pipe flow issuing perpendicularly into a cross stream, *ASME J. Fluids Engng* **104,** 493–499 (1982).
9. K. S. Chen and J. Y. Hwang, Experimental study on the mixing of one- and dual-line heated jets with a cold crossflow in a confined channel, *AIAA J.* **29,** 353–360 (1991).
10. K. N. Atkinson, Z. A. Khan and J. H. Whitelaw, Experimental investigation of opposed jets discharging normally into a cross-stream, *J. Fluid Mech.* **115,** 493–504 (1982).
11. S. V. Patankar, D. K. Basu and S. A. Alpay, Predictions of the three-dimensional velocity field of a deflected turbulent jet, *ASME J. Fluids Engng* **99,** 758–762 (1977).
12. W. P. Jones and J. J. McGuirk, Computation of a round turbulent jet discharging into a confined crossflow. In *Turbulent Shear Flow* II (Edited by L. J. S. Bradbury *et al.*). Springer, Berlin (1980).
13. J. D. Holdeman and R. Srinivasan, On modeling dilution jet flowfields, NASA TM-83708, Cleveland, OH (1984).
14. K. S. Chen and Y. R. Chang, The effects of incident angle on the mixing of opposing heated jets with a confined crossflow, National Science Council Report, NSC 82-0401-E110-034, Taiwan (1993).
15. Y. R. Chang and K. S. Chen, Measurement of opposing heated line jets discharged at an angle to a confined crossflow, *Int. J. Heat Mass Transfer* **37,** 2935–2946 (1994).
16. B. E. Launder and D. B. Spalding, Numerical computation of turbulent flows, *Comput. Math. Appl. Mech. Engng* **3,** 269–289 (1974).
17. H. Tennekes and J. L. Lumley, *A First Course in Turbulence*, pp. 146–164. MIT Press, New York (1972).
18. A. D. Gosman and F. J. K. Ideriah, TEACH-2E: a general computer program for two-dimensional turbulent recirculation flows, Report No. FM-83-2, Imperial College, London (1983).

19. S. V. Partankar, *Numerical Heat Transfer and Fluid Flow*. Hemisphere, New York (1985).
20. D. G. Sloan, P. J. Smith and L. D. Smoot, Modeling of swirl in turbulent flow systems, *Prog. Energy Combust. Sci.* **12,** 163–250 (1986).
21. S. T. Lee, Simulation of velocity and temperature fields in the combustion chamber of an incinerator, National Science Council Report, NSC 73-0401-E002-13, Taiwan (1985).